

TES OBSERVATIONS OF THE GLOBAL DISTRIBUTION OF SULFATE ON MARS. C. D. Cooper and J. F. Mustard. Dept. of Geological Sciences, Box 1846, Brown University, Providence RI 02912 (Christopher_Cooper@brown.edu).

Introduction: Sulfate was observed in the soil on Mars by the Viking and Pathfinder landers in relatively high concentrations (~5-9% SO₃) [1,2,3]. Furthermore, cohesive materials at the Viking sites had elevated sulfur contents compared to fines [2,4,5]. Together with the association of sulfur and magnesium and mixing trends with other elements, this argues for a sulfate salt component in the soils [1,5,6,7]. Being able to map the distribution and extent of sulfates and cemented materials would be useful for evaluating different mechanisms for soil formation and alteration. Spectroscopic remote sensing has the potential for mapping sulfates on Mars, but to date has found only hints of sulfate features in low spatial resolution data sets [8,9]. The Thermal Emission Spectrometer (TES) on MGS offers a new wavelength range and much higher spatial resolutions (3 km) for searching for evidence of sulfate on Mars.

Laboratory analogs of powder and cemented palagonite-sulfate mixtures indicate that sulfates on Mars should only be detectable by TES if they form coherent surfaces via cementation [10]. Sulfate-cemented crusts have relatively strong restrahlen bands at ~8.7 μm (1153 cm⁻¹) that we calculated should be detectable for surfaces where at least 5-10% of the surface is free of obscuring, loose dust. Even though the loose dust contains sulfate, it has extremely weak absorption features due to the very fine particle sizes.

Our initial results at looking at TES data [11] showed a signature that we tentatively identified an absorption in a small area on Mars that was compatible with sulfate. We have expanded on that research to look at a global dataset and carefully attempt to separate a sulfate signal from the surface of Mars.

Spectral Analysis and Deconvolution: We selected ~8.5 million TES spectra of the surface of Mars from the PDS CD-ROM archives, excluding spectra with instrument noise, poor viewing geometries, and cold surface temperatures (and hence poor signal-to-noise). The radiance spectra were converted to emissivity by dividing by a blackbody corresponding to the average of the three highest apparent brightness temperatures of a subset of bands around the Christiansen features of silicates [12]. The emissivity spectra were then averaged in groups of 6, and the averaged spectra were run through a deconvolution program.

Our deconvolution program is based on that of the TES team [13,14]. It finds the best fitting linear combination of atmospheric and surface endmembers for each emissivity spectrum over the range 233-1301 cm⁻¹ (7.68-33 μm) excluding the CO₂ band, outputting the endmembers image (Figure 1) and spectral form. Our endmember library was composed of 2 atmospheric cloud, 2 atmospheric dust, and 4 surface endmembers. The surface endmembers used (Figure 2) were the 3 used to identify hematite, Acidalia-type, and Syrtis-type surfaces by Bandfield [14]. The fourth surface endmember was the spectrum of one of our laboratory sulfate-cemented palagonitic soils. The particular sample was 12.5% MgSO₄ by weight, corresponding to 8.3% SO₃.

The endmember fractions from the deconvolution were imported into a GIS database to allow inspection of the spatial distribution of the deconvolution results on a pixel-by-pixel basis. Additionally, the deconvolution results were then gridded into a 1°x1° dataset, producing global maps of the fractional abundance of each endmember as well as two global spectral datasets with the atmos-

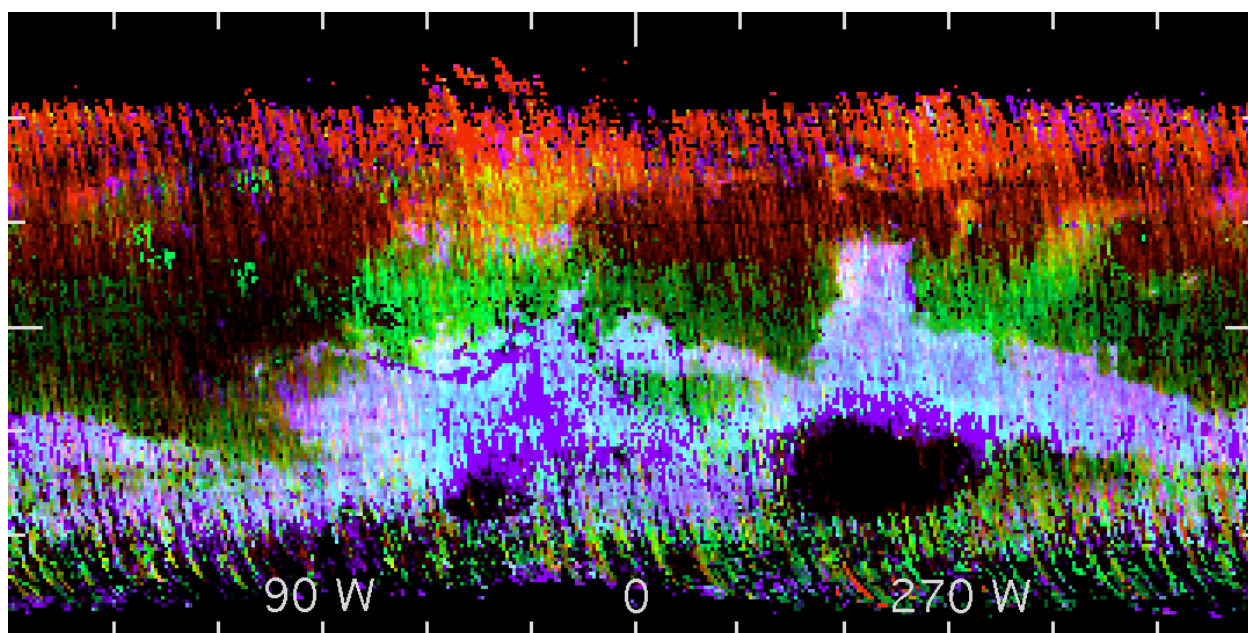


Figure 1. Image showing endmember fractions from the deconvolution of TES data gridded to 1°x1°. Red: Acidalia-type endmember, Green: Cemented sulfate endmember from laboratory sample, Blue: Syrtis-type endmember.

phere removed spectra and the modeled surface spectra.

The deconvolution results produce fractional maps of hematite, Acidalia-type, and Syrtis-type materials that correspond closely with those published by the TES team [13,14]. Further analysis of the sulfate endmember map was required to verify that the deconvolution did not include atmospheric components in the sulfate fraction. This analysis involved comparing spectra of sulfate-rich regions with the endmember set, testing for continuity across orbits and longitude, looking at correlations between endmembers, and examining spatial relationships with other endmembers. Some spurious signals were filtered out to produce the final sulfate endmember map, and further verification is ongoing.

Deconvolution Results: Spectra of regions on Mars that appear to contain cemented sulfate soils are shown in Figure 2. These spectra are the average surface spectra for $1^\circ \times 1^\circ$ spots on Mars and match the sulfate endmember quite well. Collectively, these surface spectra show an absorption centered at 1132 cm^{-1} ($8.8 \mu\text{m}$) that varies from $\sim 1\%$ to 3% in depth and approximately matches the position and shape of the absorption in the sulfate endmember. The spectra are relatively flat between the sulfate absorption and the CO_2 band and at higher wavelengths.

Abundances of sulfate range up to $\sim 8\%$ cemented sulfate, which is the percentage of the surface that is free of obscuring material (such as dust) and composed of cemented sulfate soil. Soil composition is not constrained to contain MgSO_4 *per se* [10], but merely to contain cemented sulfates. Additionally, the amount of sulfate in the cemented soil is not known, as the strength of the absorption band depends jointly on the abundance of sulfate, the degree of cementation, and the amount of material unobscured by dust [10].

The distribution of apparent cemented sulfate surfaces is shown in green in Figure 1. The sulfate fraction is not correlated with any of the other surface or atmospheric endmembers. Sulfate is primarily located in medium albedo regions (Lunae Planum, Isidis, Elysium, Southern/Western Arabia, Oxia Palus, and Northern Noachis) that previously have been postulated to be regional expanses of duricrust [15,16]. Sulfate also appears in some low albedo regions (Syrtis, part of Acidalia, and Cerberus). Finally, some sulfate is found on the shields of Olympus Mons, Alba Patera, and Ascræus Mons. The spectra in Figure 2 include examples from each region.

Implications: The sulfate regions apparently detected here are not located in topographic lows (notably absent from the northern lowlands). This argues against formation of the sulfate salts by evaporation of large-scale bodies of water. The sulfate is also not primarily centered around volcanic regions, although there is some on the Tharsis volcanoes and in Syrtis. Instead the sulfate is more widely distributed. This global pattern suggests that in these regions the sulfate in the soil was cemented by an atmospherically-driven process.

Conclusions: Deconvolution of ~ 8.5 million TES spectra using an expanded set of surface endmembers including a laboratory sample of cemented sulfate-palagonite soil has allowed the identification of regions on Mars which appear to contain sulfates. The spectral match between surface spectra and the experimental laboratory sample endmember is good and represents about 0-8% exposure of cemented sulfate soils in these regions.

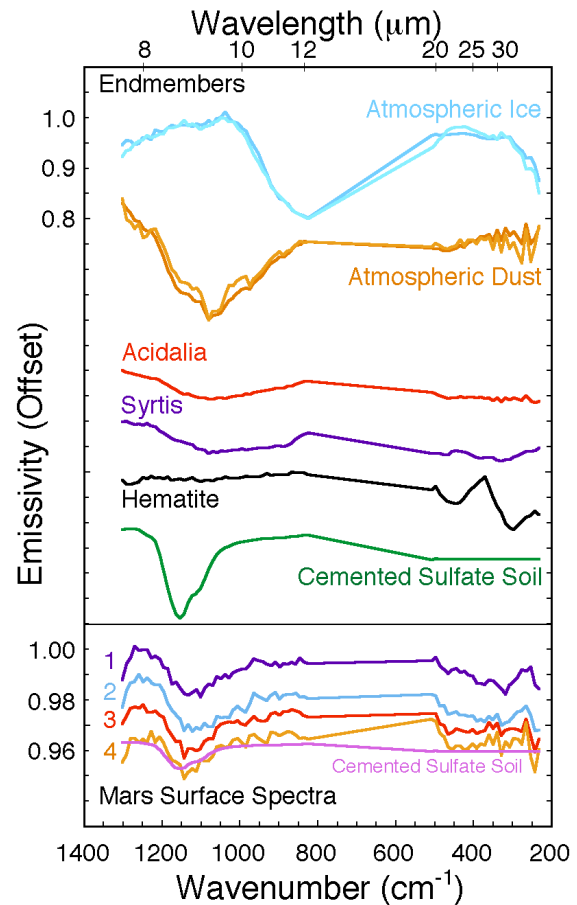


Figure 2. Spectral endmembers used in deconvolving TES spectra in top panel, surface spectra from deconvolution of TES spectra in bottom panel. 1) Arabia, 2) Isidis, 3) Lunae Planum, 4) Tharsis. Also shown is scaled sulfate endmember for comparison.

We are currently verifying that the apparent sulfate signature is not due to other causes. Because of the optical behavior of particulate and cohesive materials, if these regions do contain sulfate in the surface materials, they must be cemented. These cemented soils are located in dark red regions and dark mafic regions in the low- to mid-latitudes. Lack of correlation with topographic lows or volcanic centers argues for the formation of these cemented sulfates by atmospherically-driven processes.

References: [1] Toulmin P. *et al.* (1977) *JGR* **84**, 4625-4634. [4] Baird A.K. *et al.* (1977) *JGR* **82**, 4595-4624. [2] Clark B.C. *et al.* (1982) *JGR* **87**, 10059-10067. [3] Rieder R. *et al.* (1997) *Science* **278**, 1771-1774. [5] Clark B.C. (1993) *GCA* **57**, 4575-4581. [7] McSween H.Y. and K. Keil (2000) *GCA* **64**, 2155-2166. [8] Blaney D.L. and T.B. McCord (1995) *JGR* **100**, 14433-14441. [9] Pollack J.B. *et al.* (1990) *JGR* **95**, 14595-14627. [6] Clark B.C. and D.C. Van Hart (1981) *Icarus* **45**, 370-378. [10] Cooper C.D. and J.F. Mustard (2001) *Icarus* in review. [11] Cooper C.D. and J.F. Mustard (2000) *Eos* **81**, S293-S294. [12] Christensen P.R. (1998) *JGR* **103**, 1733-1746. [13] Smith M.D. *et al.* (2000) *JGR* **105**, 9589-9607. [14] Bandfield J.L. *et al.* (2000) *Science* **287**, 1626-1630. [15] Presley M.A. and R.E. Arvidson (1988) *Icarus* **75**, 499-517. [16] Arvidson R.E. *et al.* (1989) *JGR* **94**, 1573-1574.